# Hypersonic Interaction along a Rectangular Corner

R. J. Cresci,* S. G. Rubin,† C. T. Nardo,‡ and T. C. Lin§
*Polytechnic Institute of Brooklyn, Farmingdale, N. Y.*

**An investigation of the behavior of the three-dimensional hypersonic flow along intersecting planes has been conducted, considering both the viscous and inviscid flows and their mutual interaction. The experimental program involves measurements of surface pressures and heat-transfer rates in the vicinity of a 90° corner. The local forces and shear stresses can be obtained thereby, yielding some information on the nature of the three-dimensional boundary-layer behavior in this region. Pitot pressure contours are also obtained and utilized in the determination of the complex intersecting shock pattern in the corner. The test data was obtained at a freestream Mach number of 11.2 and a Reynolds number of $1.5 \times 10^4$/in. A theoretical analysis of the corner flow was obtained by the development of a set of equations valid throughout the boundary layer, shock wave structure, and inviscid core as previously proposed by Rubin for two-dimensional and axisymmetric flows. This analysis has been shown to be valid in the continuum merged layer and in the viscous interaction regions downstream. The theory is extended here to the three-dimensional corner configuration. Where applicable, the theoretical solutions were compared to the experiments and very good agreement was found to exist over the entire spectrum of flow variables.**

## Nomenclature

$C$ = $\bar{\mu}\bar{T}_\infty/\bar{\mu}_\infty\bar{T}$ = Chapman-Rubesin constant
$C_f$ = $2\bar{\tau}/\bar{\rho}_\infty\bar{u}_\infty^2$ = surface skin-friction coefficient
$C_F$ = $C_f/\bar{V}^{3/2}$ = normalized skin-friction coefficient
$C_p$ = $[\bar{p}/\bar{p}_\infty - 1]/\bar{\chi}$ = normalized pressure coefficient
$C_H$ = $St/\bar{V}^{3/2}$ = normalized heat-transfer coefficient
$H$ = stagnation enthalpy
$k$ = coefficient of thermal conductivity
$\bar{L}$ = $\gamma M_\infty^3/Re_\infty$ = reference length
$M$ = Mach number
$p$ = pressure
$q$ = surface heat transfer rate
$Re_x$ = $\bar{\rho}\bar{u}\bar{x}/\bar{\mu}$ = Reynolds number based on $x$
$Re_\infty$ = $\bar{\rho}_\infty\bar{u}_\infty/\bar{\mu}_\infty$ = freestream unit Reynolds number
$S_t$ = $q_w/\bar{\rho}_\infty\bar{u}_\infty(H_\infty - H_w)$ = Stanton number
$\bar{T}$ = temperature
$u$ = $\bar{u}/\bar{u}_\infty$ = nondimensional velocity in the $x$ direction
$\bar{u}$ = physical velocity in the $x$ direction
$v$ = $\bar{v}/\bar{u}_\infty\delta$ = nondimensional velocity in the $y$ direction
$\bar{v}$ = physical velocity in the $y$ direction
$\bar{V}$ = $\bar{\chi}/M_\infty^2$ = rarefaction parameter
$w$ = $\bar{w}/\bar{u}_\infty\delta$ = nondimensional velocity in the $z$ direction
$\bar{w}$ = physical velocity in the $z$ direction
$x$ = $\bar{x}/\bar{L}$ = nondimensional $x$ coordinate
$\bar{x}$ = physical coordinate in the streamwise direction
$y$ = $\bar{y}/\bar{\delta}$ = nondimensional $y$ coordinate
$\bar{y}$ = physical coordinate along vertical surface normal to $x$ axis
$z_s$ = two-dimensional shock displacement thickness
$z$ = $\bar{z}/\bar{\delta}$ = nondimensional $z$ coordinate
$\bar{z}$ = physical coordinate along horizontal surface normal to $x$ axis
$\gamma$ = ratio of specific heats
$\delta$ = $(1/\gamma^{1/2}M_\infty)$ = reference number
$\delta'$ = physical boundary-layer thickness
$\bar{\delta}$ = $\delta\bar{L}$ = reference length
$\zeta$ = $\bar{z}/\bar{z}_s = \bar{z}$ coordinate normalized with respect to the shock layer thickness
$\bar{\rho}$ = density
$\bar{\mu}$ = coefficient of viscosity
$\sigma$ = Prandtl number
$\bar{\tau}$ = $\bar{\mu}(\partial\bar{u}/\partial\bar{y})$ = shear stress
$\bar{\chi}$ = $M_\infty^3(C/Re_{\infty_{\bar{x}}})^{1/2}$ = viscous-inviscid interaction parameter

### *Subscripts*

$e$ = conditions external to boundary layer
$s$ = stagnation conditions
$t$ = Pitot conditions
$w$ = conditions evaluated at the surface
$z \to \infty$, $2 - D$ = flat plate conditions
$\infty$ = freestream conditions
2 = conditions behind a normal shock

### *Superscript*

$(\bar{\ })$ = physical flow variables

Received January 16, 1969. This research was supported by the Air Force Office of Scientific Research under Contract AF 49(638)-1623, Project No. 9781-01. Special thanks are due to NASA for support given under the NASA Predoctoral Traineeship Program. Part of this work is based on a dissertation submitted to the Polytechnic Institute of Brooklyn by T. Lin in partial fulfillment of the requirements for the degree of Doctor of Philosophy (Astronautics).

* Assistant Director of Gas Dynamics Laboratory. Member AIAA.
† Associate Professor of Aerospace Engineering. Associate AIAA.
‡ NASA Trainee.
§ Research Fellow.

## I. Introduction

An investigation of the detailed behavior of three-dimensional hypersonic flow along intersecting planes has been conducted for freestream conditions corresponding to the strong interaction and merged layer regimes. This problem, in addition to its basic scientific interest, is directly applicable to lifting configurations traveling at high velocities and high altitudes. Although the general problem of flow along a corner has been studied quite extensively in the past, as is evidenced by the comprehensive review of Ref. 1, there is not a great deal of information available in the regime of viscous-inviscid interaction. Theoretical treatments of the boundary-layer flow have been restricted to uniform external flow conditions,[2-4] whereas even for low supersonic velocities it has been shown both theoretically[5] and experimentally[6] that the outer inviscid flow is highly nonuniform in the corner region.

As a result, most of the information that has been obtained concerning corner flows has relied heavily on experimental data due to the difficulties connected with a theoretical treatment of the problem by standard techniques, i.e., by

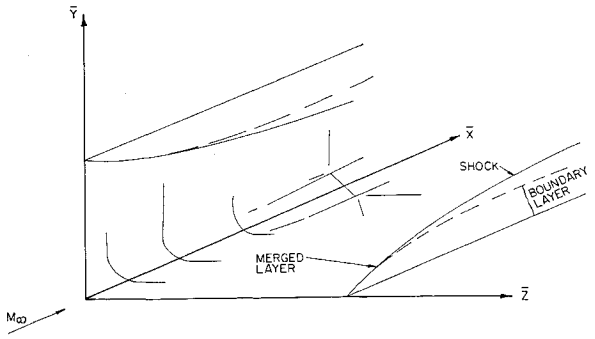


**Fig. 1 Flow system and physical coordinates.**

matching a three-dimensional boundary-layer flow with a highly nonuniform inviscid flow in which strong shock waves may be present.

Recently, a new technique has evolved for analysing high-Mach number, low-density flows over slender bodies having sharp leading edges.[7-9] Therein it is shown that a single set of equations valid throughout the disturbed flow, from the body to the freestream, represents a uniformly valid first approximation to the Navier-Stokes equations. With the boundary conditions applied at the surface and in the freestream, the "matching" of the boundary layer, inviscid flow, and outer compressive shock structure is no longer necessary. The shock formation and configuration for complex geometries is generated by a numerical solution of the equations. Although this is a distinct advantage even for two-dimensional or axisymmetric flow, it is most essential for the analysis of the three-dimensional geometry considered here. No distinct assumptions are required to treat the leading edge merged flow or the strong and weak interaction regions further downstream.

Previous results for two-dimensional[7-9] and axisymmetric[8] geometries are in good agreement with the available experimental data. The first application to a three-dimensional geometry was the flow over a finite span flat plate.[8]

The present paper presents the results of a combined experimental and theoretical program concerning the hypersonic, strong interaction flow in a 90° corner formed by two sharp, flat plates aligned with the freestream. A schematic of the flow system is shown in Fig. 1 along with the prescribed coordinate system. A viscous layer starting near the leading edge forms the continuum "merged layer"; the strong interaction regime appears downstream with a discrete boundary layer, inviscid region, and shock wave. In the corner region the two layers which form on each of the plates merge together and it is this region in particular that is examined here.

The experimental study was conducted at a freestream Mach number of 11.2 and a Reynolds number of $1.5 \times 10^4$/in. Data taken consist of surface pressures and heat-transfer rates along the surface at various distances from the corner, and also pitot pressure and total temperature surveys in cross planes corresponding to values of $\bar{\chi} = 2.5$ and 5.0. Shock shapes and some indication of the boundary-layer behavior can be inferred from these measurements.

The theoretical analysis corresponding to these freestream conditions is performed using the three-dimensional analysis described in Refs. 7 and 8 and discussed here in Sec. III. Numerical solutions are obtained by an explicit finite difference marching procedure, made possible by the parabolic nature of the governing equations. The flow far from the plate intersection is also obtained by an independent two-dimensional calculation for comparison purposes.

## II. Experimental Apparatus

The facility used for the present test program is a Mach 12 (nominal) variable Reynolds number blowdown tunnel; the air supply and heating system consists of high-pressure air storage banks and a pebble bed heater with the tunnel exhausting into a vacuum sphere. Figure 1 shows a schematic of the flow configuration which corresponds to the test model; this is the same as used in Ref. 10; further details of the model and probe design can be found in Ref. 11. Each run duration is on the order of 3–4 sec, thus providing an essentially constant model surface temperature during the test. For the range in stagnation temperatures achieved (1650–1800°R), the wall to stagnation temperature ratio was between 0.30 and 0.33.

Surface heat-transfer rates were obtained using thin plates with thermocouples spotwelded to the unexposed surface. For the plate thickness and range of aerodynamic heat rates obtained, the uniform temperature distribution across the plate permitted the heat-transfer rate to be computed from the back-side temperature history.

Stagnation temperature profiles are obtained using open tip thermocouples. The response of the thermocouple wire (0.001 in. diam) is sufficiently rapid to achieve the adiabatic wall temperature well within the run duration. No corrections are made on the raw data to convert from adiabatic wall to stagnation temperature since, 1) the scatter in the measured data is greater than the error incurred in neglecting the correction, and 2) all the data is normalized with respect to the free stream stagnation temperature which is obtained from the same type of probe. This normalization will tend to eliminate (or at least decrease) the over-all error. On the basis of repeatability and the method of data reduction, the over-all accuracy of the temperature data is believed to be within ±5%.

Pitot pressure profiles are obtained with standard type, blunt probes mounted on a movable rake. In order to determine the shock location within the desired degree of accuracy, the probes used have an o.d. of 0.060 in. and an i.d. of 0.045 in. This was found to be the smallest tube size that could be used with good response in the test times available. Since the measured pressure level extended over a range of three orders of magnitude between the surface and the freestream, several different types of pressure sensing instruments were necessary. In the vicinity of the surface, where the pressure is on the order of the free stream pressure, Hastings type, heated thermopile, high-vacuum gages are used; for pressures between 5 and 40 mm of mercury, variable reluctance type diaphragm transducers are used, whereas in regions adjacent to intersecting shock waves, the Pitot pressures are sufficiently high to require the use of Statham strain gauge transducers. Whenever the transducer type was changed, several points in the profile were overlapped to assure continuity of data obtained by the different instruments. The over-all accuracy of the pressure measurements is ±5%.

Alignment of the model in the tunnel is quite critical since even a small angularity can produce a significant change in the shock location. Both plates were mechanically aligned to within ±10′ of zero angular deflection with respect to the tunnel walls; this was checked by comparing the surface heat-transfer and pressure measurements obtained on both plates. Although these measurements agreed quite well, there is still sufficient misalignment to alter the two-dimensional shock locations by a few percent, as may be noted in the Pitot profile data. Even though this does create some asymmetry about the bisecting plane, it is not considered sufficient to alter the general flow behavior in the corner region.

## III. Theoretical Analysis

The theoretical model to be used here is analogous to that presented in Ref. 7, where a detailed description of the two-dimensional flow analysis appears. The extension to axisymmetric and three-dimensional flows is given in Ref. 8.

The theory is based on the assumption that the entire shock layer is very thin, so that for slender bodies the surface normal gradient is much larger than either of the gradients in the plane of the surface; this is true throughout the entire shock layer, including the outer compressive shock region. If the ratio of normal to tangential variations is denoted by $\delta^{-1}$, a first approximation to the Navier-Stokes equations is obtained by an expansion in $\delta^2$; terms of order $\delta^2$ are neglected except in the energy equation where $u \equiv 1$ in the outer portion of the disturbed flow and a second-approximation is required.[7] In addition, a second parameter $\Delta^2 = T_{\text{ref}}/\gamma M_\infty^2$ appears in the expanded equations. $T_{\text{ref}}$ is representative of the magnitude of the local temperature. It is shown that $\Delta^2 < 0.05$ in the cold wall limit and $\Delta^2 < 0.12$ for adiabatic conditions.[7] Therefore, in order to simplify the system of equations and reduce calculation times, $\Delta^2$ is assumed to be a small parameter. The neglect of terms of order $\Delta^2$ leads to the omission of the streamwise pressure gradient in the leading approximation. The consistancy of this assumption is discussed in Ref. 7. Terms of order $(\delta/\Delta)^2$ are retained throughout. They become small near the wall in the strong interaction region but remain of order one in the outer shock structure. Based on these considerations, the equations that describe the corner flow are

Continuity:

$$(\rho u)_x + (\rho v)_y + (\rho w)_z = 0$$

$x$ Momentum:

$$\rho u u_x + \rho v u_y + \rho w u_z = (\mu u_y)_y + (\mu u_z)_z$$

$y$ Momentum:

$$\rho u v_x + \rho v v_y + \rho w v_z = -p_y + \tfrac{4}{3}(\mu v_y)_y + (\mu v_z)_z + (\mu u_y)_x - \tfrac{2}{3}(\mu u_x)_y + (\mu w_y)_z - \tfrac{2}{3}(\mu w_z)_y$$

$z$ Momentum:

$$\rho u w_x + \rho v w_y + \rho w w_z = -p_z + \tfrac{4}{3}(\mu w_z)_z + (\mu w_y)_y + (\mu u_z)_x - \tfrac{2}{3}(\mu v_y)_z - \tfrac{2}{3}(\mu u_x)_z + (\mu v_z)_y$$

Energy:

$$\rho u T_x + \rho v T_y + \rho w T_z = -(\gamma - 1)p(u_x + v_y + w_z) + (\gamma/\sigma)(\mu T_y)_y + (\gamma/\sigma)(\mu T_z)_z + \gamma(\gamma - 1)M_\infty^2 \mu(u_y^2 + u_z^2) + \tfrac{4}{3}\mu(\gamma - 1)(v_y^2 + w_z^2 - v_y w_z) + \mu(\gamma - 1) \times (w_y + v_z)^2$$

State:

$$p = \rho T$$

$\rho$, $p$, $T$, and $u$ are nondimensionalized with their respective freestream values, $\mu$ with $\mu_\infty M_\infty$, $v$, and $w$ with $U_\infty \delta$, $x$ with $\bar{L}$, and $y$ and $z$ with $\bar{\delta}$. $\delta = \bar{\delta}/\bar{L} = (\gamma^{1/2} M_\infty)^{-1}$ and $\bar{L} = \gamma M_\infty^3 (\mu_\infty/\rho_\infty U_\infty)$. The Sutherland viscosity law, modified for low temperatures, and constant values of $\gamma = 1.4$ and $\sigma = 0.75$ are used throughout.

Slip boundary conditions are enforced at the surface, with symmetry across the diagonal;

$$y = 0,\ z > 0: \quad v = 0,\ T = T_w + [2\gamma/(\gamma + 1)](\lambda/\sigma)T_y$$
$$u = \lambda u_y$$
$$w = \lambda[w_y + 3(8\pi T)^{-1/2} T_z]$$

The lateral creep effect ($T_z$), on the slip velocity ($w$) is rather small, always less than 10%. This effect might prove more significant at higher freestream Mach numbers.

Across $y = z$: $u$, $\rho$, $T$ are symmetric, $v(y,z) = w(z,y)$. Since solutions are obtained numerically, these conditions are enforced by proper reflection across the diagonal and the equality of $v$ and $w$ along the diagonal becomes a check on the finite-difference system of equations. If freestream conditions are reached below the diagonal they are invoked in lieu of the symmetry conditions.

The initial conditions are uniform freestream values except at the surface where slip conditions prevail. Due to the parabolicity of the governing equations (only the streamlines are real characteristics) the effects of initial conditions rapidly decay so that they are no longer apparent (less than 5% deviation) when the rarefaction parameter $\bar{V} = 0.4$ or $\bar{\chi} = 50$.¶ At this location, the boundary-layer assumption, $\delta \ll 1$, is also quite acceptable. Therefore, we would expect that the solution presented herein is valid for $\bar{\chi} < 50$.

Solutions are obtained by an explicit finite difference calculation on the CDC 6600 computer. For a given streamwise location, the computation is initiated at the corner and extends outward for increasing values of $y$. Once freestream conditions, to within $10^{-3}$, are attained or the plane of symmetry is reached, the calculation moves outward one row in the lateral or $z$ direction. This process continues until two-dimensional flow profiles are obtained, i.e., flow properties vary in the lateral direction by less than $10^{-3}$. These two-dimensional results were identical with those obtained from an independent two-dimensional calculation.

The three-dimensional computation is about one hundred and fifty times slower than that for two-dimensional flow. This is due primarily to the large number of required mesh points, although a factor of three is dictated by increased stability requirements. For this reason the three-dimensional analysis was terminated at $\bar{V} = 0.25$, $\bar{\chi} = 30$. At this point, the two-dimensional results were within 3% of their strong interaction values and comparison with the experimental data in the strong interaction region was possible. The flow region $0.25 < \bar{V} < 0.4$ corresponds to the end of the merged layer.[7] The calculation takes 40 min to reach $\bar{V} = 0.34$, but 2 hr for $\bar{V} = 0.25$. For the two-dimensional computation it takes 7 min to reach $\bar{V} = 0.06$, $\bar{\chi} = 8$. A mesh width $\Delta y = \Delta z = 0.08$ was prescribed. This corresponds to somewhat less than one freestream mean free path. The effect of mesh size on the calculation is discussed in Refs. 7–9. A decrease in the mesh width leads to a negligible change in the inner shock layer, although for strong shocks the shock structure is not predicted accurately for $\bar{V} < 0.3$ until a sufficient number of points lie within the shock wave.[8] Smaller mesh widths were not used, since the computation time was already quite long. Therefore, the shock structure portion of the flow near the corner may have errors as large as 15% in peak pressure and density for $\bar{V} = 0.25$. In the two-dimensional flow, the shock is weaker and the deviations are less than 10%. Our primary concern here is the comparison with surface and interior shock layer measurements for which the smaller mesh size would alter the computed values by less than 2%.** The streamwise step size is determined by stability considerations; throughout the calculation $\Delta x < 10^{-5}$.

## IV. Presentation and Discussion of Results

The analytical results for the strictly two-dimensional calculations are compared first with the experimental data obtained at a large lateral distance from the corner ($\bar{z} \to \infty$). Figure 2, for example, shows the ratio of the local surface static pressure to freestream static pressure at several test Reynolds numbers as indicated, and for various streamwise locations on the plate. The data is plotted as a function of $\bar{\chi}$ and compared to various theories. The weak interaction theory of Lees and Probstein[12] is included as well as the strong interaction analyses of Chan[13] and Bertram.[14] The present analysis is also shown and the agreement is seen to

¶ A 20% error can be expected at $\bar{V} = 0.5$ or $\chi = 63$.

** See addendum to Ref. 8.

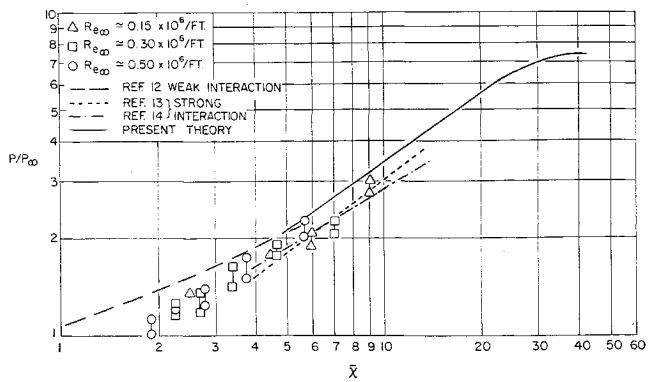


**Fig. 2 Flat plate pressure distribution ($\bar{Z} \to \infty$).**

be reasonable over the entire range of $\bar{\chi}$. Figure 3 presents the corresponding heat transfer data in terms of the local Stanton number for the same conditions. In addition, some experimental data obtained for similar freestream Mach numbers from Ref. 15 are also included. The predictions

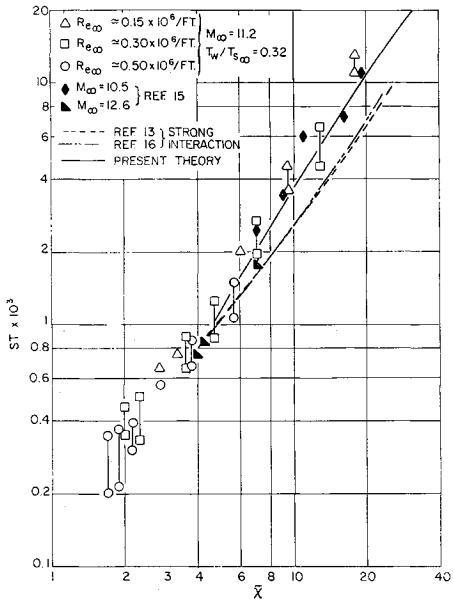


**Fig. 3 Flat plate heat transfer ($\bar{Z} \to \infty$).**

of the strong interaction analyses of Lees[16] and Chan[13] are computed for the current test conditions and are seen to underestimate the heat transfer in the strong interaction region by as much as 30%, whereas the present analysis represents a good mean value through the experimental data.

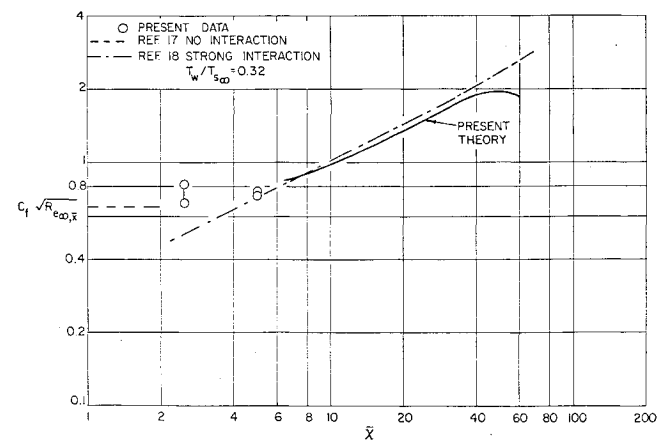


**Fig. 4 Flat plate skin friction ($\bar{Z} \to \infty$).**

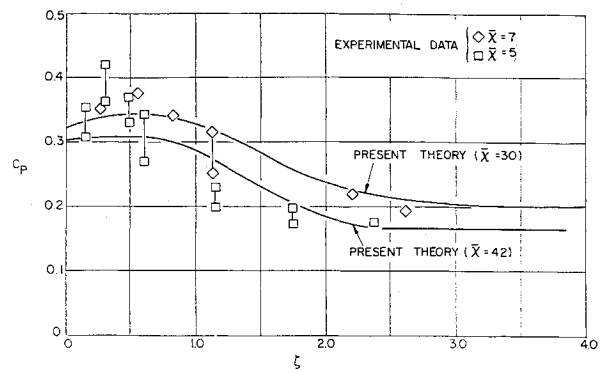


**Fig. 5 Normalized surface pressure.**

This difference is apparently due to the additional sliding friction term included in the surface heat transfer and resulting from the slip velocity at the wall. At lower values of $\bar{\chi}$ where the slip velocity vanishes, both the experimental data and all the analyses are seen to converge; however, at the higher values of $\bar{\chi}$ this discrepancy can be significant. The skin-friction coefficient for the two-dimensional flow is presented in Fig. 4. This data resulted from Preston tube measurements and was obtained only at the two values of $\bar{\chi}$ at which the complete flowfield profiles were taken. Again the present analysis, as well as the analyses of Eckert[17] and Li and Nagamatsu,[18] are included for comparison. The present theory is observed to compare quite favorably at higher values of $\bar{\chi}$ with the strong interaction theory, and at lower $\bar{\chi}$ it approaches the boundary-layer predictions of Eckert. The over-all trends, therefore, indicate that the analysis is valid from the merged layer region well into the weak interaction regime.

Having obtained satisfactory agreement with the two-dimensional results, the more interesting three-dimensional calculation and experimental data are compared in Figs. 5–13. In Fig. 5, the pressure coefficient is plotted for a given value of $\bar{\chi}$ as a function of lateral distance ($\bar{z}$) away from the corner. In order to compare the results at several different values of $\bar{\chi}$, the pressure ratio was normalized with respect to $\bar{\chi}$ and the lateral coordinate was normalized with respace to the local two-dimensional shock layer thickness. Although the corner analysis was only carried downstream to a $\bar{\chi}$ of 30, a comparison of the results shows quite good quantitative agreement over the entire range of $\bar{\chi}$. For example, the overshoot in pressure is seen to increase as the strong interaction parameter ($\bar{\chi}$) decreases from 42 to 30. The same trend is observed in the experimental data where this parameter varies from 7 to 5. Moreover, even over this wide range of the interaction parameter the agreement between the measured and computed pressure distribution is quite re-

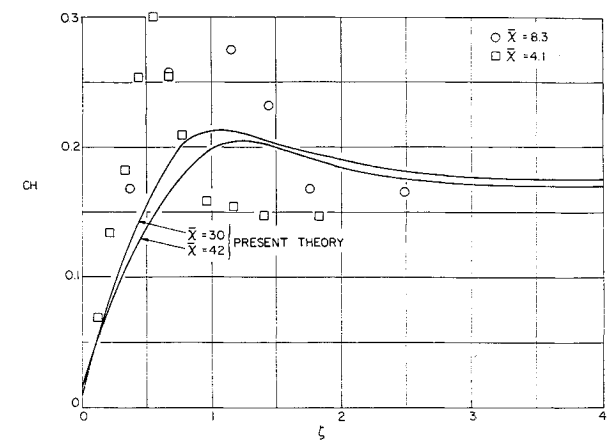


**Fig. 6 Normalized heat transfer.**

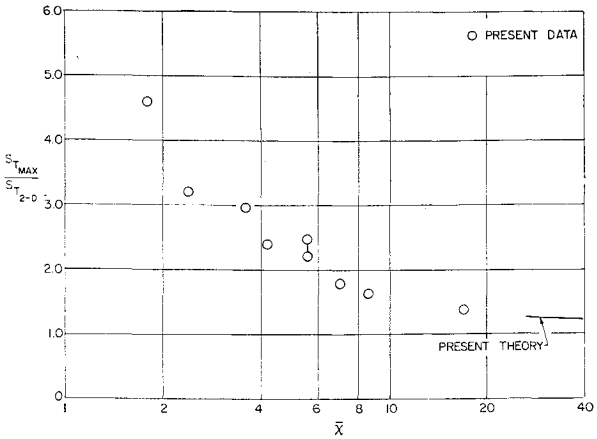


**Fig. 7 Heat-transfer maximum.**

markable. A similar distribution of heat-transfer coefficient is shown in Fig. 6, where local overshoots occur once more. Here it is seen that the peak value of the heat transfer achieved in the corner increases in magnitude and moves closer to the corner (in nondimensionalized coordinates) as the interaction parameter decreases. This trend is also observed in the experiments. In this instance, however, it is apparent that the peak value of the normalized heat-transfer coefficient is varying quite rapidly with $\bar{\chi}$ in contradistinction to the lack of variation of the maximum normalized pressure coefficient. In order to see how this trend develops, the ratio of the peak value of heat-transfer coefficient divided by the local two-dimensional value thereof was plotted as a function of the strong interaction parameter. This is shown in Fig. 7 along with the corresponding theoretical analysis. In addition, it is significant to observe that one can achieve values of heat transfer in the corner which are as much as five times as high as the flat plate value for lower values of $\bar{\chi}$. A distribution of skin-friction coefficient is shown in Fig. 8, and the same trends are observed here; i.e., the peak increases in magnitude and moves closer to the corner (in terms of local shock layer thickness) as the distance downstream from the leading edge is increased.

In addition to the surface parameters which were discussed, several flowfield measurements were obtained at two different values of the interaction parameter $\bar{\chi}$. The theoretical Pitot pressure contours obtained for $\bar{\chi} = 30$ are shown in Fig. 9. A peak in Pitot pressure is seen to occur in the vicinity of the shock wave at the plane of symmetry and the contours themselves are seen to develop an inflected shape in the corner region. When this is compared to the experimental Pitot pressure profiles shown in Fig. 10, some similarities are observed, although there are still some significant differences

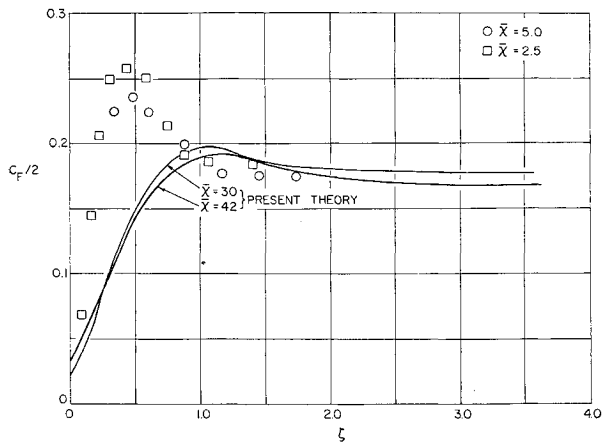


**Fig. 8 Normalized skin friction.**

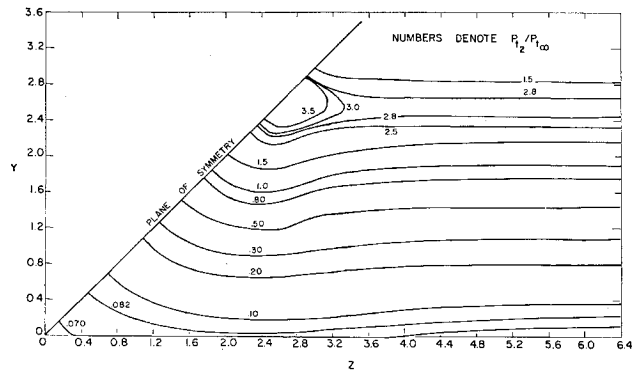


**Fig. 9 Theoretical Pitot pressure contours in corner region at $\bar{\chi} = 30$.**

which are probably due to the low value of $\bar{\chi}$ for the experiments ($\bar{\chi} = 5$). In the corner region the shock is seen to bifurcate in the region of intersection of the two-dimensional shock waves and a peak value of the Pitot pressure ratio occurs in this region. In addition, one finds a significant inflection in the Pitot contours as well as a very close spacing of these contour lines. This seems to indicate a branch of

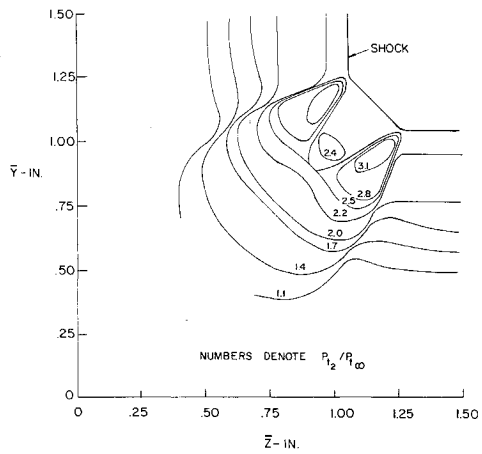


**Fig. 10 Experimental Pitot pressure contours in corner region at $\bar{\chi} = 5.0$.**

the shock wave which is propagating down toward the viscous layer. In Fig. 11, the theoretical isobars in the corner region are presented. However, since no static pressure data was obtained, there is no comparison available for this case. Figures 12 and 13 show the theoretical and experimental contours of total temperature in the corner region. Again there is a remarkable similarity in the results, the major difference being that the distortion of the lines are much more pronounced for lower values of $\bar{\chi}$. This is consistent with the greatly increased values of heat transfer achieved in the corner region for low values of the interaction parameter.

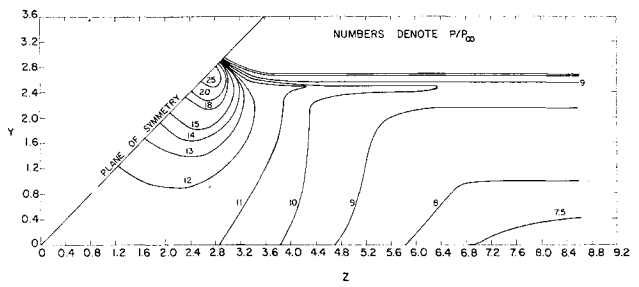


**Fig. 11 Theoretical isobars in corner region at $\bar{\chi} = 30$.**

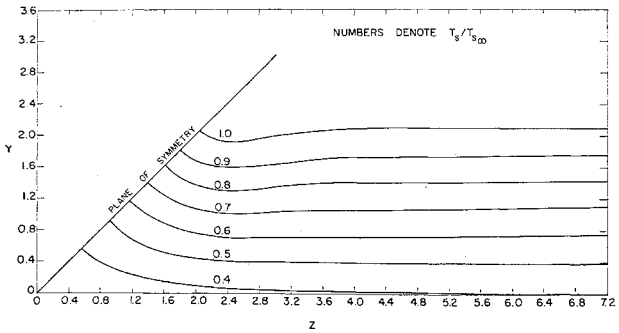


**Fig. 12 Theoretical total temperature contours in corner region at $\bar{\chi} = 30$.**

## V. Concluding Remarks

A series of experiments have been performed in the viscous-inviscid interaction region in a hypersonic flow aligned with a corner intersection and have been compared to a merged layer analysis for the same freestream and surface conditions. For the two-dimensional conditions the theory and experiments were compared over the entire interaction range and excellent agreement is seen to occur.

For the flow in the corner, the computations were not carried out as far downstream as the experiments were performed. However, despite this apparent limitation, the surface pressure, heat-transfer, and skin-friction data agree quite well both in the weak and strong interaction regimes. Flowfield measurements were obtained for both total temperature and Pitot pressure and were also found to agree quite well qualitatively with the analytical results.

On the basis of this somewhat detailed comparison it is concluded that the analytical technique presented herein can be utilized in a wide variety of three-dimensional interaction problems. In some cases the computations may take a relatively long time, however, this analysis is at present the only technique that can be satisfactorily used for these general three-dimensional flow configurations.

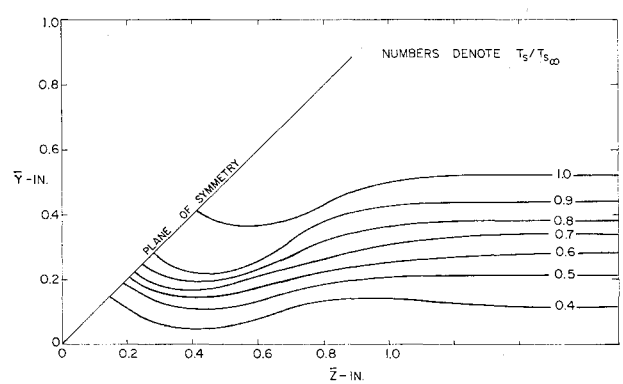


**Fig. 13 Experimental total temperature contours in corner region at $\bar{\chi} = 5.0$.**

## References

[1] Stainback, P. C. and Weinstein, L. M., "Aerodynamic Heating in the Vicinity of Corners at Hypersonic Speeds," TN D-4130, Nov. 1967, NASA.

[2] Carrier, G. F., "The Boundary Layer in a Corner," *Quarterly of Applied Mathematics*, Vol. IV, No. 4, Jan. 1947, pp. 367–370.

[3] Bloom, M. H. and Rubin, S. G., "High-Speed Viscous Corner Flow," *Journal of the Aerospace Sciences*, Vol. 28, No. 2, Feb. 1961, pp. 145–157.

[4] Rubin, S. G., "Incompressible Flow Along a Corner," *Journal of Fluid Mechanics*, Vol. 26, Pt. 1, Sept. 1966, pp. 97–110.

[5] Wallace, J. and Clarke, J. H., "Uniformly Valid Second-Order Solutions for Supersonic Flow Over Cruciform Surfaces," *AIAA Journal*, Vol. 1, No. 1, Jan. 1963, pp. 179–185.

[6] Charwat, A. F. and Redekopp, L. G., "Supersonic Interference Flow along the Corner of Intersecting Wedges," *AIAA Journal*, Vol. 5, No. 3, March 1967, pp. 480–488.

[7] Rudman, S. and Rubin, S. G., "Hypersonic Viscous Flow over Slender Bodies Having Sharp Leading Edges," *AIAA Journal*, Vol. 6, No. 10, Oct. 1968, pp. 1883–1889.

[8] Rubin, S. G. et al., "Hypersonic Interactions near Sharp Leading Edges," *AIAA Journal*, Vol. 7, No. 9, Sept. 1969, pp. 1744–1751.

[9] Cresci, R. J., Rubin, S. G., and Nardo, C. T., "Hypersonic Flow in Rectangular and Non-Rectangular Corners," *Proceedings of the AGARD Specialists' Meeting on "Hypersonic Boundary Layers and Flow Fields,"* London, England, May 1–3, 1968.

[10] Cresci, R. J., "Hypersonic Flow Along Two Intersecting Planes," PIBAL Report 895, AFOSR 66-0500, March 1966, Polytechnic Instit. of Brooklyn; also presented at the 1966 Heat Transfer and Fluid Mechanics Institute, Univ. of Santa Clara, Calif., June 22–24, 1966.

[11] Nardo, C. T. and Cresci, R. J., "Hypersonic Interactions in Corners of Various Angles." PIBAL No. 69-1, Jan. 1969, Polytechnic Institute of Brooklyn.

[12] Lees, L. and Probstein, R. F., "Hypersonic Viscous Flow over a Flat Plate," Rept. 195, Contract AF 33(038)-250, April 1952, Aeronautical Engineering Lab., Princeton Univ.

[13] Chan, Y.-Y., "Integral Methods in Compressible Laminar Boundary Layers and their Application to Hypersonic Pressure Interactions," CR-284, Sept. 1965, NASA.

[14] Bertram, M. H. and Blackstock, T. A., "Some Simple Solutions to the Problem of Predicting Boundary-Layer Self-Induced Pressures," TN D-798, April 1961, NASA.

[15] Hall, J. G. and Golian, T. C., "Shock Tunnel Studies of Hypersonic Flat-Plate Air Flows," Rept. AD-1052-A-10, Dec. 1960, Cornell Aeronautical Lab.

[16] Lees, L., "On the Boundary-Layer Equations in Hypersonic Flow and Their Approximate Solutions," *Journal of the Aerospace Sciences*, Vol. 20, No. 2, 1953, p. 143.

[17] Eckert, E. R. G., "Survey on Heat Transfer at High Speeds," TR 54-70, 1954, Wright Air Development Center.

[18] Li, T. Y. and Nagamatsu, H. T., "Hypersonic Viscous Flow on Noninsulated Flat Plate," *Proceedings Fourth Midwestern Conference on Fluid Mechanics*, Purdue Engineering Research Series 128, 1955, pp. 273–287.